JACS
JOURNAL OF THE AMERICAN CHEMICAL SOCIETY
Communication
pubs.acs.org/JACS

Alkyne-Functionalized Superstable Graphitic Silver Nanoparticles for Raman Imaging

Zhi-Ling Song,[†] Zhuo Chen,*[,†] Xia Bian,[†] Li-Yi Zhou,[†] Ding Ding,[†] Hao Liang,[†] Yu-Xiu Zou,[†] Shan-Shan Wang,[†] Long Chen,[§] Chao Yang,[†] Xiao-Bing Zhang,*[,†] and Weihong Tan*[,†,‡]

[†]Molecular Sciences and Biomedicine Laboratory, State Key Laboratory for Chemo/Biosensing and Chemometrics, College of Chemistry and Chemical Engineering, College of Biology and Collaborative Innovation Center for Molecular Engineering and Theronastics, Hunan University, Changsha 410082, China

[‡]Department of Chemistry and Department of Physiology and Functional Genomics, Center for Research at Bio/nano Interface, Shands Cancer Center, UF Genetics Institute and McKnight Brain Institute, University of Florida, Gainesville, Florida 32611-7200, United States

[§]Faculty of Sciences, University of Macau, Av. Padre Tomás Pereira Taipa, Macau, China

Supporting Information

ABSTRACT: Noble metals, especially gold, have been widely used in plasmon resonance applications. Although silver has a larger optical cross section and lower cost than gold, it has attracted much less attention because of its easy corrosion, thereby degrading plasmonic signals and limiting its applications. To circumvent this problem, we report the facile synthesis of superstable AgCu@graphene (ACG) nanoparticles (NPs). The growth of several layers of graphene onto the surface of AgCu alloy NPs effectively protects the Ag surface from contamination, even in the presence of hydrogen peroxide, hydrogen sulfide, and nitric acid. The ACG NPs have been utilized to enhance the unique Raman signals from the graphitic shell, making ACG an ideal candidate for cell labeling, rapid Raman imaging, and SERS detection. ACG is further functionalized with alkyne-polyethylene glycol, which has strong Raman vibrations in the Raman-silent region of the cell, leading to more accurate colocalization inside cells. In sum, this work provides a simple approach to fabricate corrosion-resistant, water-soluble, and graphene-protected AgCu NPs having a strong surface plasmon resonance effect suitable for sensing and imaging.

Noble metal nanoparticles have gained considerable attention due to their outstanding optical properties. In particular, gold nanoparticles (Au NPs), which possess strong plasmonic properties through their long electronic relaxation, have been applied in surface-enhanced Raman scattering (SERS).[1] Actually, silver has larger optical cross section and lower cost than gold,[2] making it a more suitable material for plasmon resonance applications. However, Au is often preferred because its surface is less susceptible to corrosion. More specifically, Ag is easily affected by such ambient factors as O_2 or H_2S, forming silver oxide or silver sulfide on the surface, thereby degrading plasmonic signals and limiting applications.[3]

To maintain the excellent properties of Ag, many efforts to reduce corrosion have been explored.[4] Cubukcu reported that the surface of a Ag nanostructure passivated with a monolayer of graphene on a quartz substrate could not be penetrated by sulfur compounds. Kalyanaraman found that a Ag−Co bimetallic structure had more stable plasmonic characteristics than pure Ag on a quartz substrate. Although their approaches retained the plasmonic properties of Ag, the preparation processes were complicated, and because of the solid substrate, the Ag nanostructures were insoluble in water, which also limited their applications, especially in bioimaging and biosensing.

One possible approach for fabricating superstable and soluble Ag NPs involves encapsulating them in appropriate shells. Indeed, graphene could be an ideal shell material based on its superior chemical stability, mechanical capacity, optical properties, thermal stability, and electrical conductivity.[5] More importantly, graphene exhibits admirable impermeability for small molecules, even helium atoms,[6] and has emerged as one of the most extensively studied nanomaterials.[7] High-quality graphene has been grown onto the surfaces of different transition metal substrates (Cu, Ni, Pd, Pt, and Co)[8] by chemical vapor deposition (CVD). While it is difficult to grow graphene on the surface of Ag because of its weak catalytic activity, the use of inexpensive Cu could overcome this problem, since Cu catalyzes the growth of graphene and Ag and Cu form good alloys. Here we report the use of CVD to grow a few layers of graphene on the surface of AgCu NPs to fabricate superstable graphitic Ag NPs. The formation of few-layer graphene on the surface of Ag NPs was catalyzed by Cu at high temperature. Sulfur compounds and oxides could not penetrate the graphene to contaminate the surface of Ag, and ACGs efficiently maintained the excellent plasmonic properties of Ag, even in the presence of hydrogen peroxide, hydrogen sulfide, and nitric acid.

Such stable ACGs could be utilized for various plasmon resonance applications, such as Raman imaging for intracellular NP localization. SERS Raman imaging as an emerging field has generated a lot of interest and applications. Raman-based methods offer a powerful analytical tool that extends the possibilities of vibrational spectroscopy with extremely high sensitivity and multiplexing capabilities to solve more chemical

Received: July 23, 2014
Published: September 18, 2014

   dx.doi.org/10.1021/ja507368z | J. Am. Chem. Soc. 2014, 136, 13558−13561

and biochemical problems.[1] Nanoparticle cellular interactions are increasingly under investigation to support applications such as targeted imaging and diagnostics, drug delivery, and heat- or radiation-based therapeutics.[9] In these cases, localization of the NPs within the cell is critical to the intended therapeutic function. The stable plasmon resonance effect has been utilized for enhancing the unique Raman signals from the graphitic shell, making ACG an ideal candidate for cell labeling, rapid Raman imaging, and SERS detection. However, the Raman signals of ACGs often overlap with those from cellular components, making the signals difficult to distinguish. It is well known that alkynes possess strong vibrations in the Raman-silent region of the cell.[10] To solve this problem, (4-phenylethynyl)benzylamino polyethylene glycol (alkyne-PEG) was synthesized and conjugated to the graphitic surface of ACGs through simple, but strong, $\pi-\pi$ interactions. By combining alkynyl and graphitic Raman signals, ACGs were accurately colocalized inside the cells.

The ACG structurally consists of a AgCu alloy core encapsulated in a graphitic shell (Figure 1a). By utilizing

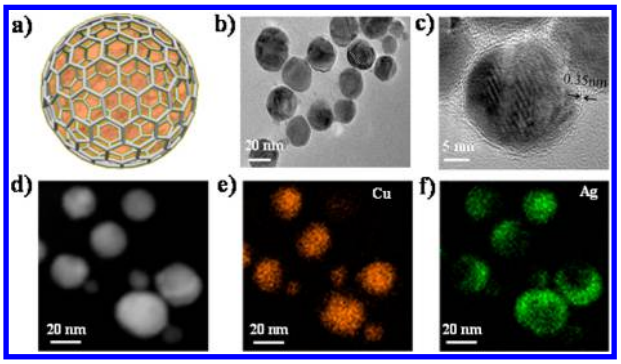

Figure 1. Advanced structural analysis of ACGs. (a) Schematic diagram of ACG, including a AgCu core and a graphitic shell. (b) TEM image of ACGs around 25 nm. (c) HR-TEM image of ACGs, with the arrows showing the 0.35 nm lattice constant of the graphitic layer. (d–f) STEM images of ACG nanostructures and the elemental map. Left, dark field; middle, Cu; right, Ag.

transmission electron microscopy (TEM, Figure 1b) and high-resolution TEM (HR-TEM, Figure 1c), the morphology and composition of ACG were characterized, clearly exhibiting the formation of the core–shell structure. The ACG demonstrated a size distribution with an average diameter ~25 nm. The space between the shell layers was ~0.35 nm, consistent with the interlayer distance in graphite, suggesting that the AgCu core was encapsulated by a graphitic shell. The existence of AgCu alloy was further proved by scanning transmission electron microscopy (STEM, Figure 1d–f). Formation of the AgCu alloy was believed to contribute to the growth of the graphitic shell. More TEM images were obtained and energy dispersive spectrometry and selected area electron diffraction were performed (Figure S1); all tests confirmed the core–shell structure of ACGs. The plasmonic properties of ACGs could be modulated by changing the Ag/Cu ratio, as verified by inductively coupled plasma mass spectrometry (Table S1) and UV/vis spectrophotometry (Figure S2).

We next assessed the corrosion resistance of ACGs. UV/vis characterization was utilized to monitor the plasmonic properties and morphological changes under different conditions. For comparison, bare Ag NPs were synthesized.[11] Temporal changes of aqueous solutions of bare Ag NPs and ACGs (Figure 2a,b) after adding 220 mM H_2O_2 were investigated. The localized

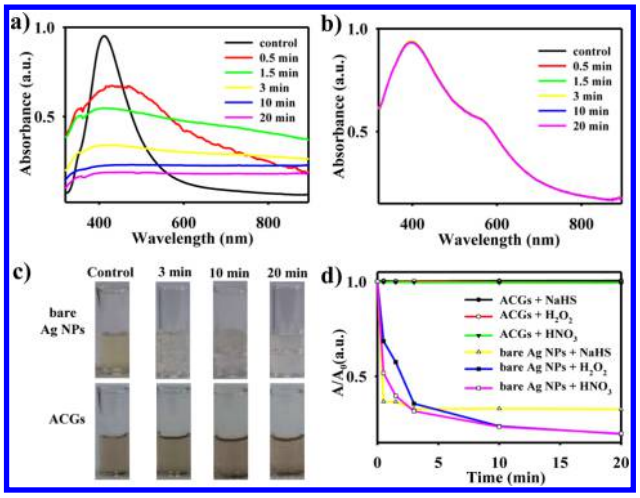

Figure 2. UV/vis spectra of bare Ag NPs (a) and ACGs (b) after adding 220 mM H_2O_2 for various times. (c) Digital photos of bare Ag NPs and ACGs suspensions mixed in 220 mM H_2O_2 for various times. (d) A/A_0 (relative absorbance intensity, where A_0 and A are the optical absorbance without and with the presence of 0.15 mM NaHS, 220 mM H_2O_2, or 75 mM HNO_3, respectively) at different time points.

surface plasmon resonance (LSPR) peak around 410 nm of bare Ag NPs decreased quickly within 20 min, while peaks around 400 and 600 nm of ACGs showed few changes. Figure 2c shows digital photos of bare Ag NPs and ACGs solution after addition of 220 mM H_2O_2 for different incubation times. Bare Ag NPs produced bubbles and became colorless because of the violent reaction between Ag and H_2O_2. In contrast, no obvious changes were observed in the ACGs, which benefited from the protective graphitic shells. Different concentrations of H_2O_2 were also used to further investigate the stability of bare Ag NPs and ACGs solution. The minor changes in UV/vis spectra and color of the ACGs with time indicate the outstanding ability of ACGs to resist oxidation compared to bare Ag NPs (Figure S3).

Apart from oxides, the Ag surface can also be damaged by H_2S and HNO_3, dramatically diminishing plasmonic properties and rendering Ag unreliable for applications. We further investigated the ability of ACGs to resist H_2S and HNO_3 corrosion. Figure 2d shows the temporal changes of the spectra for ACGs and bare Ag NPs after adding H_2O_2, NaHS, and HNO_3. For bare Ag NPs, the intensity of the LSPR absorbance peak decreased significantly, while ACGs showed no changes in position or intensity in LSPR peaks. ACGs exhibited considerable resistance against corrosion from H_2O_2, H_2S, and HNO_3 as a result of protective graphitic shells. Other concentrations of NaHS and HNO_3 were also investigated, and ACGs demonstrated superior stabilities (Figures S4 and S5). Bare AgCu NPs demonstrated lower stability compared to ACGs (Figure S6).

The cytotoxicity of ACGs was investigated through MTS assay. ACGs exhibited good biocompatibilities. Negligible inhibition of proliferation was observed in MCF-7 breast cancer cells stained with ACGs (Figure S7).

Next, these stable ACGs were utilized to enhance the distinctive Raman signals from the graphitic shells, demonstrating that ACG makes a good Raman tag for cell imaging and an excellent SERS substrate for bioimaging and biosensing. ACG has two prominent Raman vibration bands, a graphitic carbon (G) peak around 1590 cm^{-1} and a disordered (D) peak around 1330 cm^{-1} (Figure 3a). The relatively high Raman D peak of ACG is attributed to increasing intensity for smaller crystallite

dx.doi.org/10.1021/ja507368z | J. Am. Chem. Soc. 2014, 136, 13558–13561

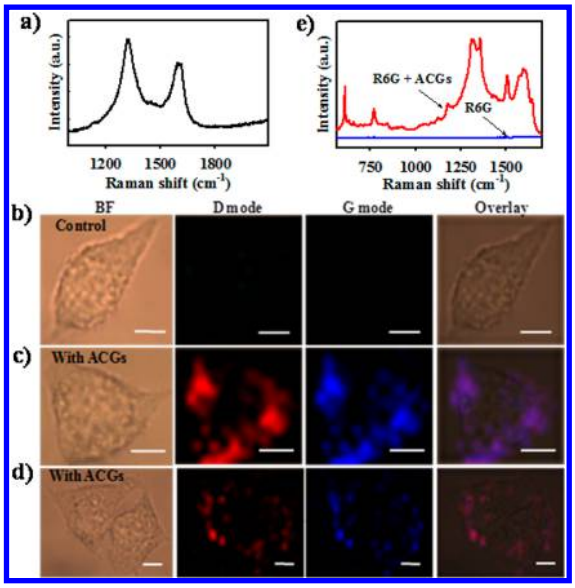

Figure 3. SERS with the ACGs. (a) Raman spectrum of the ACGs with the G and D bands of graphitic shell. High-resolution Raman image of MCF-7 cells treated without (b) and with (c) ACGs using 1 s integration/pixel. (d) Rapid Raman image of MCF-7 cells treated with ACGs using 0.1 s integration/pixel. (e) Raman spectra of 20 μM R6G with (red) and without (blue) ACGs. BF, bright field; scale bar, 10 μm.

size.[12] The AgCu core significantly enhanced the Raman signal of the graphitic shell. Compared to other organic Raman-active molecules, ACG has enormous Raman scattering cross sections ($\sim 10^{-21}$ cm^2 sr^{-1} molecule^{-1}) as a graphitic nanomaterial,[13] and it is more stable because of its inorganic structure. Both the D and G bands could be utilized to image cells and tissues.

Figure 3b,c shows the Raman images of MCF-7 cells stained without and with ACGs, respectively (1 s integration time per pixel). Strong Raman signals were observed in the ACGs stained cells. All Raman signals in Figure 3c are distributed throughout the cellular cytoplasm, with no signal emerging from the nucleus, indicating the cell distribution of ACGs. Strong and rapid enhancement of Raman signals by the core−shell structure is a key advantage of using ACGs as Raman probes for cell imaging. For example, one Raman image could be acquired in several minutes (Figure 3d, 0.1 s integration/pixel), a remarkable reduction from the tens of minutes taken by previous methods (1−2 s integration/pixel). Similar to Figure 3c, Raman signals in Figure 3d were also localized in the cellular cytoplasm. Based on strong Raman scattering, only a few seconds were needed to acquire one Raman image by using the global imaging mode with an expanding laser beam. Figure S8 shows the global imaging of the ACGs stained cells, and the entire image was obtained in only 10 s. Compared to fluorescence imaging, the Raman signals in the cells have good spatial resolution as a result of the narrow full width at half-maximum of the Raman peak and the unbleached Raman signals. This represents a potentially useful tool for monitoring endocytosis processes of ACGs inside cells. Further utilizing the ACGs as Raman tags for cell and tissue imaging has also been investigated. To improve the selectivity, cancer cell specific aptamers are conjugated onto the ACG surface through the $\pi-\pi$ stacking (Figure S9). The aptamer-functionalized ACGs exhibit good targeting imaging (Figures S10 and S11), which indicates great potential in clinical applications.

ACGs were also excellent substrates for the enhancement of Raman signals by orders of magnitude of molecules adsorbed on NPs. The key virtue of using ACGs as a SERS substrate is the higher detection sensitivity and vast practical applications by the strongly enhanced Raman signals. On the other hand, the chemically inert thin shell of ACGs can prevent direct interaction between adsorbates and bare AgCu cores, which could help to prevent photocarbonization of signal molecules or nearby impurity molecules under strong or prolonged laser irradiation[14] while retaining the significant Raman enhancement effect. Rhodamine 6G (R6G) was used as a model molecule for detection and to determine SERS enhancement (Figure 3e). When ACGs were added to the R6G solution, the Raman signals were significantly enhanced. ACGs were also able to quench R6G background fluorescence through the fluorescence resonance energy transfer (FRET) process,[8] significantly improving the detection signal-to-noise ratio. The Raman detection with ACGs also demonstrates superior stability as compared to bare Ag NPs (Figure S12), which is critical for a SERS detection substrate.

Raman microscopy is capable of detecting specific vibrational stretches, as well as imaging cells. This property makes possible the intracellular localization of NPs to realize their intended therapeutic role. However, numerous Raman signals often overlap with those from cellular components, making the signals difficult to distinguish. Alkyne possesses a strong vibration in the Raman-silent region of the cell (1800−2800 cm^{-1}).[10]

Functionalization of ACGs with alkyne molecules could help to more accurately localize ACGs in the cells. This could be achieved by conjugating alkyne with PEG molecules. The alkyne molecule diphenylacetylene, with a high Raman scattering cross section,[10] was efficiently synthesized and conjugated on the PEG chain (Figure 4a). Alkyne-PEG is also a good surfactant, having a

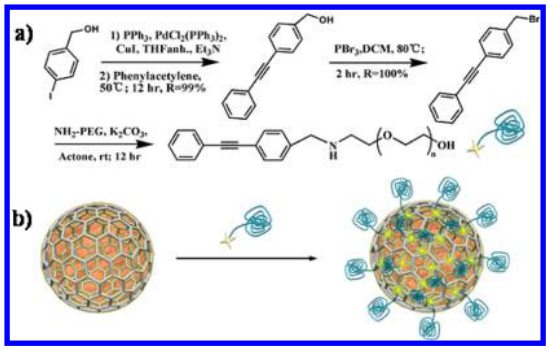

Figure 4. Preparation of alkyne-PEG-modified ACGs. (a) Synthesis procedure of alkyne-PEG. (b) Schematic illustration of the alkyne-PEG functionalization of ACGs.

hydrophilic PEG chain and a hydrophobic diphenylacetylene tail, which could be functionalized on the surface of ACGs through strong $\pi-\pi$ stacking to help solubilize ACGs.

Figure 4b illustrates the alkyne-PEG-functionalized ACG. The graphitic shell acts as an ideal platform to adsorb alkyne-PEG molecules. Meanwhile, the AgCu core could simultaneously enhance the Raman signals from both the graphitic shell and alkyne-PEG through the SERS effect, which, in turn, could be utilized to colocalize ACGs inside cells. Figure 5a (red curve) shows the Raman spectrum of alkyne-PEG, with a strong and narrow alkyne peak around 2220 cm^{-1}. The efficiency of adsorbing alkyne-PEG on ACGs was also clearly demonstrated (Figure 5a, black curve). Three distinct Raman peaks could be observed: the peak at 1330 cm^{-1} mainly comes from the graphitic shell, while the peak at 2220 cm^{-1} is assigned to C≡C stretching of alkyne-PEG, and the peak at 1590 cm^{-1} is their mutual peak.

dx.doi.org/10.1021/ja507368z | J. Am. Chem. Soc. 2014, 136, 13558−13561

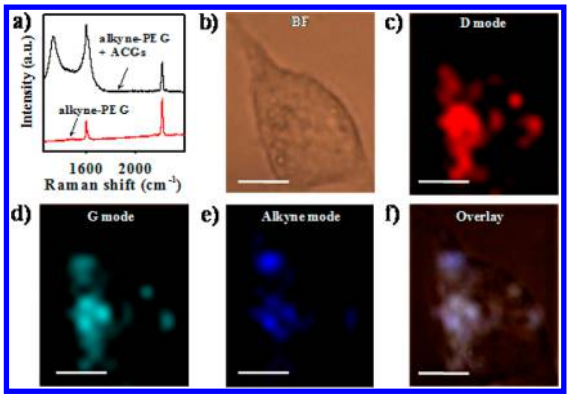

Figure 5. Cell imaging with alkyne-PEG-functionalized ACGs. (a) Raman spectra of alkyne-PEG with (black) and without (red) ACGs. (b–f) Raman image of MCF-7 cells treated with alkyne-PEG-modified ACGs using 1 s integration/pixel. BF, bright field; scale bar, 10 μm.

The results clearly demonstrate the successful functionalization of alkyne-PEG on the surface of ACGs.

Alkyne-PEG-functionalized ACGs exhibited excellent Raman imaging of cells. High-resolution Raman images of MCF-7 cells treated with functionalized ACGs are shown in Figure 5b–f. All three modes, i.e., D, G, and alkyne, were utilized for the colocalization of ACGs, demonstrating good intracellular localization capability (representative point spectra of the cell Raman images were included in Figures S13 and S14). All signals spread throughout the cell cytoplasm and accurately indicated the location of ACGs.

In summary, we have developed a simple approach that provides corrosion resistance for silver nanoparticles by protecting their surface with several layers of graphene. AgCu NPs were synthesized and successfully encapsulated with graphitic shells. Compared to bare Ag NPs, the plasmonic properties of ACGs showed almost no degradation in the presence of H_2O_2, H_2S, or HNO_3, demonstrating superior stability. ACGs showed strong Raman signals from the graphitic shell and remarkable SERS-enhancing capability from the AgCu core. Particularly worth mentioning are good water solubility, biocompatibility, and nanoscale size, making ACGs widely applicable in bioimaging.

Raman imaging of cells with ACGs was also demonstrated, using a significantly shortened imaging time as a result of the strong Raman signals of ACGs with SERS enhancement. Alkyne-PEG molecules were synthesized and functionalized on the ACG surface to realize cell imaging at the Raman-silent region. These alkyne-PEG molecules not only have large Raman scattering cross section but can also adsorb on the ACG surface through strong $\pi-\pi$ stacking interactions. After functionalization, ACGs were accurately colocalized inside the cells with the D, G, and alkyne Raman modes. In addition to cell imaging and detection, such superstable graphitic Ag NPs show promise in such bioapplications as targeted imaging and diagnostics, photothermal therapy, drug delivery, and biosensing.

■ ASSOCIATED CONTENT

Supporting Information

Procedures and additional data. This material is available free of charge via the Internet at http://pubs.acs.org.

■ AUTHOR INFORMATION

Corresponding Author

zhuochen@hnu.edu.cn; xbzhang@hnu.edu.cn; tan@chem.ufl.edu

Notes

The authors declare no competing financial interest.

■ ACKNOWLEDGMENTS

This work was financially supported by the National Key Basic Research Program of China (Nos. 2013CB932702, 2011CB911000), the Research Fund for the Program on National Key Scientific Instruments and Equipment Development (No. 2011YQ0301241402), the National Natural Science Foundation of China (NSFC 21105025, NSFC 21221003, and NSFC 21327009), the U.S. National Institutes of Health (GM079359 and CA133086), and the Hunan Innovation and Entrepreneurship Program.

■ REFERENCES

(1) Keren, S.; Zavaleta, C.; Cheng, Z.; Zerda, A.; Gheysens, O.; Gambhir, S. S. *Proc. Natl. Acad. Sci. U.S.A.* **2008**, *105*, 5844. Rycenga, M.; Xia, X.; Moran, C. H.; Zhou, F.; Qin, D.; Li, Z. Y.; Xia, Y. *Angew. Chem., Int. Ed.* **2011**, *50*, 5473. Qian, X.; Peng, X. H.; Ansari, D. O.; Yin-Goen, Q.; Chen, G. Z.; Shin, D. M.; Yang, L.; Young, A. N.; Wang, M. D.; Nie, S. *Nat. Biotechnol.* **2008**, *26*, 83. Abramczyk, H.; Brozek-Pluska, B. *Chem. Rev.* **2013**, *113*, 5766. Kneipp, K.; Kneipp, H.; Kneipp, J. *Acc. Chem. Res.* **2006**, *39*, 443.

(2) Link, S.; El-Sayed, M. A. *J. Phys. Chem. B* **1999**, *103*, 8410. Erol, M.; Han, Y.; Stanley, S. K.; Stafford, C. M.; Du, H.; Sukhishvili, S. *J. Am. Chem. Soc.* **2009**, *131*, 7480. Millstone, J. E.; Hurst, S. J.; Metraux, G. S.; Cutler, J. I.; Mirkin, C. A. *Small* **2009**, *5*, 646.

(3) Cao, W.; Elsayed-Ali, H. E. *Mater. Lett.* **2009**, *63*, 2263.

(4) Gao, C.; Hu, Y.; Wang, M.; Chi, M.; Yin, Y. *J. Am. Chem. Soc.* **2014**, *136*, 7474. Gao, C.; Lu, Z.; Liu, Y.; Zhang, Q.; Chi, M.; Cheng, Q.; Yin, Y. *Angew. Chem., Int. Ed.* **2012**, *51*, 5629. Reed, J. C.; Zhu, H.; Zhu, A. Y.; Li, C.; Cubukcu, E. *Nano Lett.* **2012**, *12*, 4090. Sachan, R.; Ramos, V.; Malasi, A.; Yadavali, S.; Bartley, B.; Garcia, H.; Duscher, G.; Kalyanaraman, R. *Adv. Mater.* **2013**, *25*, 2045.

(5) Xie, L.; Wang, H.; Jin, C.; Wang, X.; Jiao, L.; Suenaga, K.; Dai, H. *J. Am. Chem. Soc.* **2011**, *133*, 10394. Geim, A. K.; Novoselov, K. S. *Nat. Mater.* **2007**, *6*, 183. Tan, Y.; Xu, C.; Chen, G.; Liu, Z.; Ma, M.; Xie, Q.; Zheng, N.; Yao, S. *ACS Appl. Mater. Interfaces* **2013**, *5*, 2241.

(6) Bunch, J. S.; Verbridge, S. S.; Alden, J. S.; van der Zande, A. M.; Parpia, J. M.; Craighead, H. G.; McEuen, P. L. *Nano Lett.* **2008**, *8*, 2458.

(7) Yang, K.; Wan, J.; Zhang, S.; Zhang, Y.; Lee, S. T.; Liu, Z. *ACS Nano* **2011**, *5*, 516.

(8) Edwards, R.; Coleman, K. S. *Acc. Chem. Res.* **2013**, *46*, 23. Song, Z. L.; Zhao, X. H.; Liu, W. N.; Ding, D.; Bian, X.; Liang, H.; Zhang, X. B.; Chen, Z.; Tan, W. *Small* **2013**, *9*, 951.

(9) Shah, N. B.; Dong, J.; Bischof, J. C. *Mol. Pharmacol.* **2010**, *8*, 176.

(10) Lin, L.; Tian, X.; Hong, S.; Dai, P.; You, Q.; Wang, R.; Feng, L.; Xie, C.; Tian, Z. Q.; Chen, X. *Angew. Chem., Int. Ed.* **2013**, *52*, 7266. Yamakoshi, H.; Dodo, K.; Palonpon, A.; Ando, J.; Fujita, K.; Kawata, S.; Sodeoka, M. *J. Am. Chem. Soc.* **2012**, *134*, 20681. Abramczyk, H.; Waliszewska, G.; Kołodziejski, M. *J. Phys. Chem. A* **1998**, *102*, 7765. Kneipp, J.; Kneipp, H.; Kneipp, K. *Proc. Natl. Acad. Sci. U.S.A.* **2006**, *103*, 17149.

(11) Mei, Q.; Zhang, Z. *Angew. Chem., Int. Ed.* **2012**, *51*, 5602.

(12) Athanassiou, E. K.; Grass, R. N.; Stark, W. J. *Nanotechnology* **2006**, *17*, 1668.

(13) Chen, Z.; Tabakman, S. M.; Goodwin, A. P.; Kattah, M. G.; Daranciang, D.; Wang, X. R.; Zhang, G. Y.; Li, X. L.; Liu, Z.; Utz, P. J.; Jiang, K. L.; Fan, S. S.; Dai, H. *Nat. Biotechnol.* **2008**, *26*, 1285.

(14) Xu, W.; Ling, X.; Xiao, J.; Dresselhaus, M. S.; Kong, J.; Xu, H.; Liu, Z.; Zhang, J. *Proc. Natl. Acad. Sci. U.S.A.* **2012**, *109*, 9281.